NeuroImage: Clinical 31 (2021) 102736

Contents lists available at ScienceDirect

NeuroImage: Clinical

journal homepage: www.elsevier.com/locate/ynicl

Brain iron assessment in patients with First-episode schizophrenia using quantitative susceptibility mapping

Man Xu [a,1], Yihao Guo [b,1], Junying Cheng [a], Kangkang Xue [a], Meng Yang [a], Xueqin Song [c], Yanqiu Feng [d,e,*], Jingliang Cheng [a,*]

[a] Department of MRI, The First Affiliated Hospital of Zhengzhou University, Zhengzhou, China
[b] MR Collaboration, Siemens Healthcare Ltd, Guangzhou, China
[c] Department of Psychiatry, The First Affiliated Hospital of Zhengzhou University, Zhengzhou, China
[d] School of Biomedical Engineering, Southern Medical University, Guangzhou, China
[e] Guangdong Provincial Key Laboratory of Medical Image Processing, Key Laboratory of Mental Health of the Ministry of Education & Guangdong-Hong Kong-Macao Greater Bay Area Center for Brain Science and Brain-Inspired Intelligence, Southern Medical University, Guangzhou, China

ARTICLE INFO

Keywords:
Schizophrenia
MRI
Brain iron
Quantitative susceptibility mapping
Grey matter nucleus

ABSTRACT

Purpose: Decreased serum ferritin level was recently found in schizophrenia. Whether the brain iron concentration in schizophrenia exists abnormality is of research significance. Quantitative susceptibility mapping (QSM) was used in this study to assess brain iron changes in the grey matter nuclei of patients with first-episode schizophrenia.

Methods: The local ethics committee approved the study, and all subjects gave written informed consent. Thirty patients with first-episode schizophrenia and 30 age and gender-matched healthy controls were included in this study. QSM and effective transverse relaxation rate (R_2*) maps were reconstructed from a three-dimensional multi-echo gradient-echo sequence. The inter-group differences of regional QSM values, R_2* values and volumes were calculated in the grey matter nuclei, including bilateral caudate nucleus, putamen, globus pallidus, substantia nigra, red nucleus, and thalamus. The diagnostic performance of QSM and R_2* was evaluated using receiver operating characteristic curve. The correlations between regional iron variations and clinical PANSS (Positive and Negative Syndrome Scale) scores were assessed using partial correlation analysis.

Results: Compared to healthy controls, patients with first-episode schizophrenia had significantly decreased QSM values (less paramagnetic) in the bilateral substantia nigra, left red nucleus and left thalamus ($p < 0.05$, FDR correction). QSM proved more sensitive than R_2* regarding inter-group differences. The highest diagnostic performance for first-episode schizophrenia was observed in QSM value of the left substantia nigra (area under the curve, AUC = 0.718, $p = 0.004$). Regional volumes of bilateral putamen and bilateral substantia nigra were increased ($p < 0.05$, FDR correction) in first-episode schizophrenia. However, both QSM and R_2* values did not show significant correlations with PANSS scores ($p > 0.05$).

Conclusion: This study reveals decreased iron concentration in grey matter nuclei of patients with first-episode schizophrenia. QSM provides superior sensitivity over R_2* in the evaluation of schizophrenia-related brain iron changes. It demonstrated that QSM may be a potential biomarker for further understanding the pathophysiological mechanism of first-episode schizophrenia.

1. Introduction

Schizophrenia is a severe psychiatric disorder that is characterized by positive symptoms (including delusions, hallucinations, and thought disorders), negative symptoms (including affective flattening, apathy and social withdrawal), and cognitive deficits (impaired working memory) (Jing et al., 2012; van Os et al., 2010). There is no consensus on the explanations of the pathophysiology of schizophrenia. Several neurotransmitter systems have been implicated in the pathophysiology of the disease (Lyne et al., 2004). The revised dopamine hypothesis

* Corresponding authors at: Department of MRI, The First Affiliated Hospital of Zhengzhou University, Zhengzhou, China (J. Cheng).
E-mail addresses: foree@163.com (Y. Feng), fccchengjl@zzu.edu.cn (J. Cheng).
[1] The first two authors contributed equally to this study.

https://doi.org/10.1016/j.nicl.2021.102736
Received 20 February 2021; Received in revised form 30 April 2021; Accepted 17 June 2021
Available online 23 June 2021

(Howes and Kapur, 2009) is one of the most influential theories on the etiology of schizophrenia. This hypothesis proposes that the multiple genetic and environmental risk factors for schizophrenia interact through one final common pathway of presynaptic striatal dopamine dysregulation. The glutamate hypothesis is also a momentous hypothesis in the pathophysiology of schizophrenia. This hypothesis emphasizes diminished activity of glutamate receptors in the glutamatergic system (Goff and Coyle, 2001). Since the glutamatergic system interacts closely with the dopaminergic system at both the neuronal circuitry level and the intracellular level (Konradi and Heckers, 2003), patients may have malfunctions in one or both systems due to the multiple forms of schizophrenia.

In the human brain, neurotransmitter synthesis and signaling depend on electron facilitation by iron (Stankiewicz et al., 2007). Iron is essential for numerous fundamental neurological processes including neurotransmitter synthesis, neuronal development, myelin production, oxygen transportation, cell proliferation and energy metabolism (Ganz and Nemeth, 2006; Hare et al., 2013; Rouault, 2013; Stankiewicz et al., 2007; Ward et al., 2014). Iron metabolism homeostasis is important for maintaining the integrity of the neurochemical circuits including monoaminergic system (Hare et al., 2013; Hyacinthe et al., 2015; Moos and Morgan, 2004), glutamatergic and gamma-aminobutyric acid (GABA) system (Ward et al., 2007). The dysregulation of iron homeostasis has been implicated in neuropsychiatric disorders (Zheng and Monnot, 2012). Excessive iron deposition could enhance free radical formation and contribute to oxidative stress (Crichton et al., 2011). Conversely, reductions in iron supply would disrupt neurodevelopment and result in long-term changes in neurotransmission (Hare and Double, 2016; Unger et al., 2007). The serum ferritin levels were reported to be significantly reduced in first-episode schizophrenia patients with prominent negative symptoms (Kim et al., 2018). However, as there are many factors that affect iron transport, uptake and storage, and serum ferritin concentrations cannot accurately reflect the brain iron content (Nielsen et al., 2000). Therefore, visualization and reliable quantitative evaluation of brain iron concentration could contribute to the investigation of pathophysiology of schizophrenia.

Magnetic resonance imaging (MRI) can non-invasively perform brain iron quantification. Effective transverse relaxation rate (R_2*) and quantitative susceptibility mapping (QSM) (Rochefort et al., 2010; Wang and Liu, 2015), calculated from the multi-echo gradient-echo (GRE) sequence, are two effective measures for iron in biological tissues. R_2* (Liu et al., 2015), which is derived by fitting the magnitude of multi-echo GRE images to an exponential function, has been applied to characterize iron concentration in the brain, and widely used for Parkinson's disease (Barbosa et al., 2015; Langkammer et al., 2010), multiple sclerosis (Khalil et al., 2009, 2011), and Huntington's disease (Cristina et al., 2015). However, R_2* can be contaminated by the macroscopic background field effects (Ropele and Langkammer, 2016). QSM, which is calculated from the phase of multi-echo GRE images, can reveal the accurate underlying susceptibility of the iron-containing tissues with reduced artifacts inherent in R_2* (Li et al., 2012a). Typically, QSM provides excellent image contrast between iron-rich grey matter (GM) nucleus and surrounding brain tissues, and also provides high sensitivity and specificity for estimating iron content (Li et al., 2011). In recent studies, QSM has become increasingly prominent in searching for a quantitative biomarker for the assessment of iron concentration. QSM studies detected significant deposition of brain iron in patients with Parkinson's disease (He et al., 2015), Huntington's disease (van Bergen et al., 2016) and multiple sclerosis (Langkammer et al., 2013), compared with healthy individuals. However, to the best of our knowledge, QSM has not been reported in patients with schizophrenia.

Previous autopsy researches and noninvasive iron-sensitive MRI studies have indicated that the brain iron concentration is not uniform (Hallgren and Sourander, 1958; Li et al., 2014; Ramos et al., 2014). The highest iron contents were detected in the deep GM nuclei (Haacke et al., 2005; Ward et al., 2014), whereas the iron contents in white matter, cortical GM and cerebellum were relatively low. These deep GM nuclei constantly generate high levels of neurotransmitters such as dopamine and glutamate to maintain the integration and transmission of signals in brain circuits (Eskreis-Winkler et al., 2017; Stuber et al., 2016). As iron serves as the cofactor in neurotransmitter biosynthesis, the functions of the GM nuclei are susceptible to changes in iron concentrations.

In the present study, QSM and R_2* mapping were used to investigate the presence of abnormal iron concentration in iron-rich deep GM nuclei of first-episode schizophrenia patients compared with healthy controls, and detect the possible correlations between QSM and R_2* values and disease severity scores.

2. Materials and Methods

2.1. Subjects

This study was approved by the local ethics committee and all subjects signed written informed consent before MR examination. A total of 35 first-episode schizophrenia patients were prospectively enrolled from Jan 2020 to Aug 2020. All patients were assessed by a psychiatrist with the Structural Clinical Interview for Diagnostic and Statistical Manual of Mental Disorders, Fourth Edition (DSM-IV) and fulfilled with the diagnostic criteria for schizophrenia in DSM-IV. All patients had not received antipsychotic medication. Clinical symptoms of patients were quantified with the Positive and Negative Syndrome Scale (PANSS). Additionally, 30 age and gender-matched healthy volunteers were recruited as healthy controls (HCs) in the same time period. Inclusion criteria for all subjects were right-handedness and age (14–40 years). General exclusion criteria included MRI contraindications, central nervous system disorders, head trauma, pregnancy, histories of systemic medical diseases, histories of substance abuse, and histories of electroconvulsive shock treatment. Additional exclusion criteria for HCs were history of any Axis I disorder in DSM-IV and first-degree relative with a psychotic disorder. Five patients were excluded due to severe motion artifacts in the MR images after the image quality inspection, thus 30 patients and 30 HCs were finally included in the study.

2.2. MRI data acquisition

The images of all participants were acquired by a 3.0 T MRI system (Discovery MR750, GE Healthcare) equipped with an 8-channel head coil. During scanning, foam padding was applied to prevent head movement and earplugs were provided to reduce the noise. A three-dimensional (3D) multi-echo GRE sequence with 8 equally spaced echoes was performed for both QSM and R_2* calculation. Imaging parameters were as follows: repetition time (TR) = 50.22 ms; first echo time (TE) = 3.67 ms; echo spacing = 5.76 ms; number of echoes = 8; flip angle (FA) = 12°; field of view (FOV) = 240 mm × 240 mm; matrix = 320 × 320; slice thickness = 2.0 mm; in-plane resolution = 0.75 × 0.75 mm^2; acquisition time = 6min45s. In addition, a 3D T1-weighted BRAVO sequence was used for measuring subject intracranial volume with the following parameters: TR = 8.17 ms; TE = 3.18 ms; inversion time (TI) = 450 ms; FA = 12°; sagittal acquisition with FOV = 256 mm × 256 mm; matrix = 256 × 256; slice thickness = 1.0 mm; slices = 188. Conventional MR images, including T2-weighted fluid-attenuated inversion recovery sequence and T2-weighted fast spin echo sequence were acquired to exclude brain structural abnormalities and cerebrovascular diseases.

2.3. Image processing

QSM was reconstructed from the 3D multi-echo GRE images. First, the wrapped total field map was generated from multi-echo magnitude and phase images using a non-linear least squares fitting method, and then the image was unwrapped with a Laplacian-based approach (Schofield and Zhu, 2003). Subsequently, the tissue field was revealed

by excluding the background fields with the Laplacian boundary value (LBV) algorithm (Zhou et al., 2014). Finally, the tissue field was inverted to QSM maps using morphology enabled dipole inversion (MEDI) algorithm (Liu et al., 2011b). In addition, R_2* maps were calculated from the multi-echo magnitude images using auto-regression on linear operations (ARLO) algorithm (Pei et al., 2015). The flow chart of the QSM and R_2* calculation is shown in Fig. 1.

After QSM and R_2* maps were reconstructed from all subjects, the regions of interest (ROIs) of deep GM nuclei were manually segmented on the reconstructed QSM maps using ITK-SNAP (Yushkevich et al., 2006) software by two neuroradiologists who were blinded to the diagnosis of subjects. The ROIs included the bilateral caudate nucleus (CN), putamen (PUT), globus pallidus (GP), substantia nigra (SN), red nucleus (RN), and thalamus (THA). Nucleus with obvious boundary was delineated in multiple adjacent slices, and then eroded inward by 2 pixels in each slice to reduce the partial volume effects. The resulting 3D models were used as masks to obtain the mean QSM and R_2* values for each ROI. The volume of each ROI was determined by multiplying the number of voxels within the entire structure with the voxel size. To eliminate the effect of different brain sizes across subjects, the individual normalized ROI volume was calculated by: normalized ROI volume = original ROI volume × (group mean intracranial volume / subject intracranial volume) (Chen et al., 2019).

2.4. Statistical analyses

All statistical analyses were performed with IBM SPSS software version 22 and MedCalc software version 19.6.3. A p value < 0.05 was considered as statistically significant. The normal distribution of data was initially tested using the Kolmogorov-Smirnov test. The independent two-sample t-test and the Chi-square test were performed to assess the inter-group differences of age and gender, respectively. The inter-rater reliability of manual segmentation was calculated using absolute intraclass correlation coefficient (ICC) of QSM values in each ROI. One-way ANCOVA test was used to assess the inter-group differences of normalized ROI volumes, with patient age and gender as covariates. To estimate the differences of QSM value and R_2* value between two groups in each ROI, one-way ANCOVA test was employed, with ROI volumes, age and gender as covariates. Post hoc false discovery rate (FDR) correction was employed for multiple comparison correction. The area under the curve (AUC) of the receiver operating characteristic (ROC) curve was used to evaluate the diagnostic performance of QSM and R_2* for the regions that showed intergroup differences. To investigate the relationship of the QSM and R_2* values with PANSS scores, partial correlation analysis was performed in regions that showed intergroup differences, with patient age and gender as covariates.

3. Results

3.1. Demographic and clinical data analyses

Demographic characteristics of the participants and PANSS scores of the first-episode schizophrenia patients are summarized in Table 1. There were no significant differences between patients and HCs in age ($t = 1.098$, $p = 0.277$) and gender ($\chi^2 = 1.111$, $p = 0.292$).

3.2. Comparison of mean regional measurements between groups

Two representative axial slices of QSM from a first-episode schizophrenia patient are shown in Fig. 2. The targeted deep GM nuclei were hyperintense and had clear shape, demonstrating that it was feasible to identify and manually segment subcortical structures on QSM map directly. ICCs for all the segmented GM nuclei in Table 2 were greater than 0.8, indicating excellent absolute agreement between raters.

The QSM values, R_2* values and volumes of the nuclei are reported in Table 3 and Fig. 3. Compared to HCs, a significant decrease (less paramagnetic) in QSM values was found in bilateral SN, left RN and left THA in first-episode schizophrenia patients ($p < 0.05$, FDR correction). With respect to R_2* values, no significant differences between two groups were found. The normalized ROI volumes of bilateral PUT and bilateral

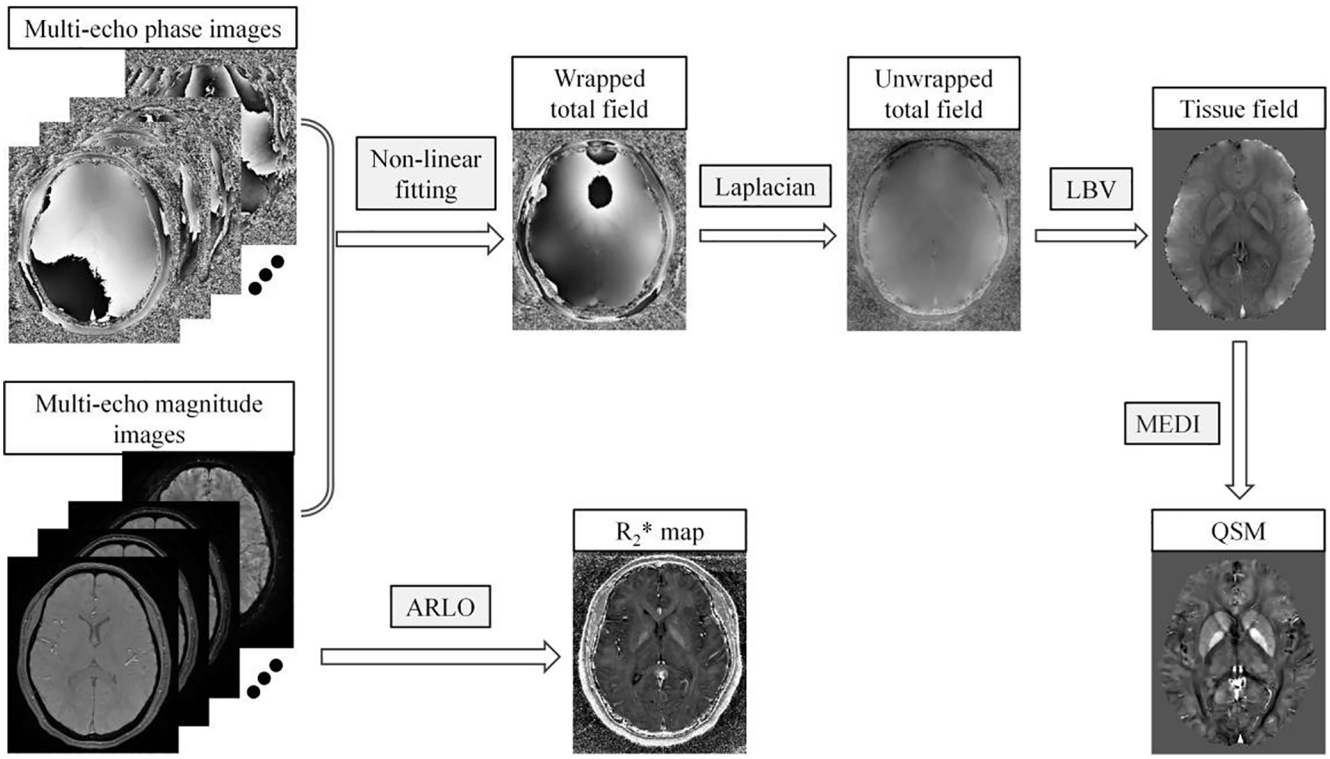

Fig. 1. The flow chart of the QSM and R_2* calculation. LBV, Laplacian boundary value; MEDI, morphology enabled dipole inversion; ARLO, auto-regression on linear operations.

Table 1
Demographic and clinical characteristics of first-episode schizophrenia patients and healthy controls.

		FES	HCs	Statistics	*p* value
Sex (M/F)		14/16	10/20	$\chi^2 = 1.111$	0.292
Age (years)		19.47 ± 5.39	20.90 ± 4.69	$t = 1.098$	0.277
PANSS	Positive	18.82 ± 5.04	/	/	/
	Negative	21.01 ± 4.94	/	/	/
	General psychopathology	37.64 ± 6.20	/	/	/
	Total	77.45 ± 10.39	/	/	/

Values are given in means ± standard deviations. FES, first-episode schizophrenia; HCs, healthy controls; PANSS, Positive and Negative Syndrome Scale.

SN were significantly increased in patient group ($p < 0.05$, FDR correction), compared with HCs. Fig. 4 shows representative QSM maps of two same age individuals, a first-episode schizophrenia patient and a HC subject, indicating lower susceptibility in the deep GM nuclei in the patient.

3.3. Diagnostic performance of QSM and R_2*

Fig. 5 shows the results of ROC curve analyses of QSM and R_2* values. QSM values were differentiated between the first-episode schizophrenia patients and HCs in the left SN (AUC = 0.718, p = 0.004), right SN (AUC = 0.679, p = 0.017), left RN (AUC = 0.672, p = 0.022), and left THA (AUC = 0.678, p = 0.018). R_2* failed to differentiate patients from HCs in the left SN (AUC = 0.621, p = 0.107), right SN (AUC = 0.608, p = 0.152), left RN (AUC = 0.619, p = 0.114), and left THA (AUC = 0.614, p = 0.128). QSM in the left SN provided the highest diagnostic performance.

3.4. Correlation of PANSS scores and MRI measurements

Table 4 summarizes the results of the partial correlation analyses in first-episode schizophrenia patients. There were no statistically significant correlations between PANSS scores and QSM and R_2* values.

4. Discussion

In the present study, we utilized QSM and R_2* mapping to quantify specific regional iron concentrations in GM nuclei of patients with first-episode schizophrenia and HCs. The results of this study showed significantly decreased QSM values in bilateral SN, left RN, and left THA in patients, while no significant inter-group differences of R_2* values were found in these nuclei. ROI volumes in bilateral PUT and bilateral SN were significantly increased in patients. QSM in the left SN provided the highest diagnostic performance. Therefore, QSM could be a potential iron-related biomarker for the mechanism of first-episode schizophrenia.

The majority of brain iron consists of paramagnetic ferric iron stored in ferritin, and ferrous iron in the oxygen transporter hemoglobin (Beard and Connor, 2003). Previous autopsy studies have concluded that the dominant source of the magnetic susceptibility in the deep grey matter is the ferric iron stored in glial ferritin. These studies validated QSM by demonstrating that the quantitative susceptibility value is highly correlated with the ferritin iron content measured by Perls' iron staining and inductively coupled plasma mass spectrometry (Langkammer et al., 2012; Sun et al., 2015; Zheng et al., 2013). The application researches of QSM method also demonstrated that QSM values in the deep GM nuclei

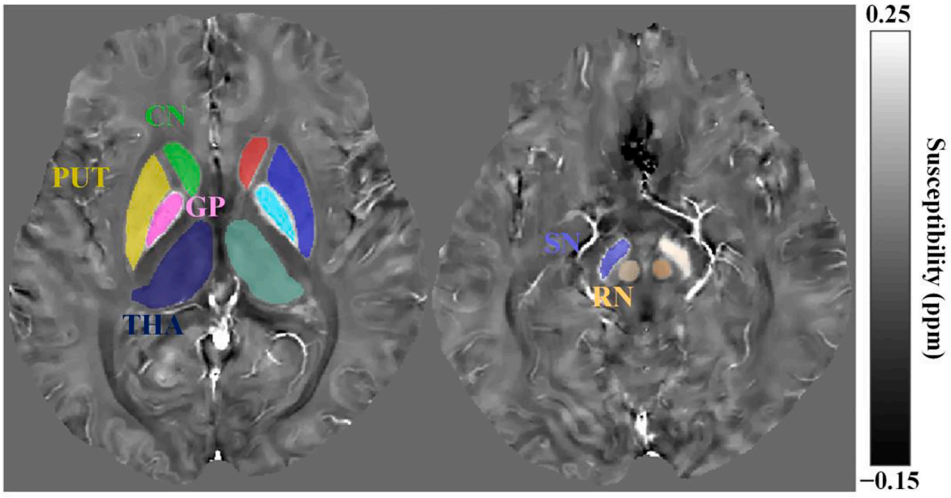

Fig. 2. Two representative axial slices of QSM images from a first-episode schizophrenia patient with color overlay of targeted deep grey matter nuclei. CN, caudate nucleus; PUT, putamen; GP, globus pallidus; SN, substantia nigra; RN, red nucleus; THA, thalamus. (For interpretation of the references to color in this figure legend, the reader is referred to the web version of this article.)

Table 2
Absolute ICCs for agreement between the raters for segmentation of the grey matter nuclei in first-episode schizophrenia patients and healthy controls.

		CN		PUT		GP		SN		RN		THA	
		Left	Right	Left	Right	Left	Right	Left	Right	Left	Right	Left	Right
ICC	FES	0.893	0.887	0.888	0.898	0.912	0.911	0.876	0.884	0.853	0.850	0.896	0.875
	HCs	0.901	0.911	0.899	0.901	0.910	0.921	0.870	0.879	0.848	0.851	0.901	0.881

ICC, intraclass correlation coefficient; FES, first-episode schizophrenia; HCs, healthy controls; CN, caudate nucleus; PUT, putamen; GP, globus pallidus; SN, substantia nigra; RN, red nucleus; THA, thalamus.

Table 3
Regional QSM, R_2* values and volumes for the first-episode schizophrenia patients and healthy controls.

		QSM Values (ppm)			R_2* Values (sec^{-1})			ROI Volumes (mL)		
		FES	HCs	p_FDR	FES	HCs	p_FDR	FES	HCs	p_FDR
CN	Left	0.045 ± 0.014	0.047 ± 0.011	0.333	19.8 ± 1.8	20.4 ± 1.8	0.339	4.6 ± 1.2	4.7 ± 1.1	0.896
	Right	0.050 ± 0.015	0.053 ± 0.013	0.635	20.0 ± 1.6	21.1 ± 1.6	0.204	5.2 ± 1.0	4.9 ± 1.0	0.534
PUT	Left	0.037 ± 0.013	0.042 ± 0.011	0.352	21.0 ± 2.1	22.2 ± 1.9	0.204	7.9 ± 1.4	7.2 ± 1.4	**0.042**
	Right	0.035 ± 0.014	0.039 ± 0.010	0.877	21.1 ± 1.9	22.2 ± 2.0	0.276	8.3 ± 1.7	7.4 ± 1.4	**0.039**
GP	Left	0.138 ± 0.029	0.153 ± 0.026	0.202	34.8 ± 5.2	36.3 ± 4.6	0.405	3.2 ± 0.6	3.0 ± 0.7	0.352
	Right	0.139 ± 0.023	0.151 ± 0.025	0.246	34.4 ± 3.7	36.4 ± 4.4	0.295	3.3 ± 0.7	3.1 ± 0.6	0.161
SN	Left	0.117 ± 0.023	0.142 ± 0.029	**0.044**	31.7 ± 3.5	33.8 ± 4.9	0.295	0.7 ± 0.2	0.6 ± 0.2	**0.024**
	Right	0.119 ± 0.032	0.140 ± 0.030	**0.044**	31.5 ± 3.5	33.3 ± 4.2	0.339	0.7 ± 0.2	0.6 ± 0.1	**0.024**
RN	Left	0.048 ± 0.024	0.067 ± 0.025	**0.044**	26.0 ± 3.1	27.7 ± 3.4	0.258	0.4 ± 0.1	0.4 ± 0.1	0.832
	Right	0.051 ± 0.029	0.065 ± 0.024	0.168	26.5 ± 3.0	27.6 ± 3.5	0.339	0.4 ± 0.1	0.4 ± 0.1	0.683
THA	Left	0.010 ± 0.005	0.014 ± 0.005	**0.048**	19.3 ± 1.2	19.8 ± 1.1	0.258	9.7 ± 1.6	9.4 ± 1.8	0.534
	Right	0.011 ± 0.005	0.013 ± 0.005	0.238	19.5 ± 1.1	20.0 ± 1.5	0.339	9.5 ± 1.8	9.7 ± 1.9	0.896

Values are given in means ± standard deviations; Bold, $p < 0.05$, significant inter-group differences after the FDR correction; FES, first-episode schizophrenia; HCs, healthy controls; CN, caudate nucleus; PUT, putamen; GP, globus pallidus; SN, substantia nigra; RN, red nucleus; THA, thalamus.

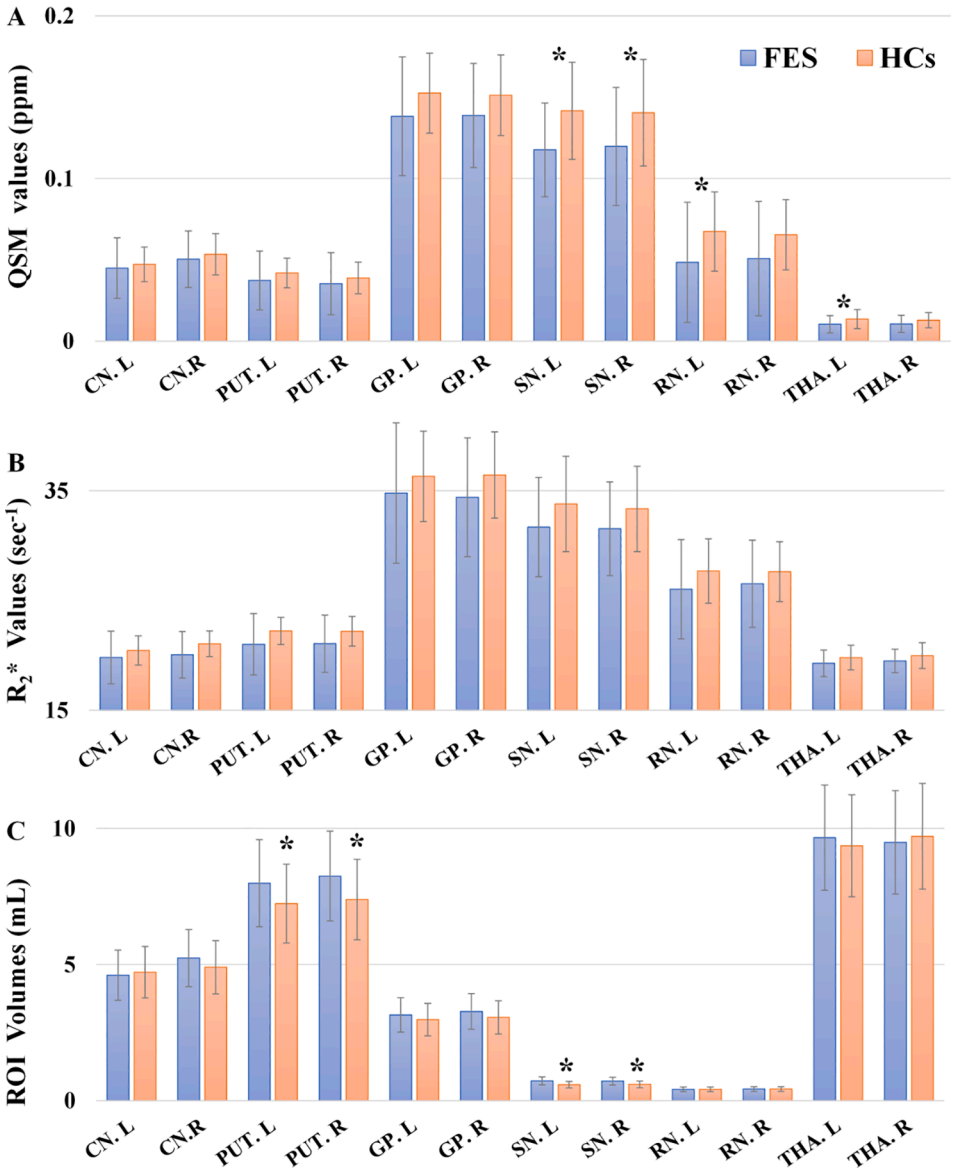

Fig. 3. Comparison of ROI-based QSM values (A), R_2* values (B) and volumes (C) between the first-episode schizophrenia patients and HCs. Asterisk (*), $p < 0.05$, significant inter-group differences after the FDR correction. FES, first-episode schizophrenia; HCs, healthy controls; CN, caudate nucleus; PUT, putamen; GP, globus pallidus; SN, substantia nigra; RN, red nucleus; THA, thalamus. (For interpretation of the references to color in this figure legend, the reader is referred to the web version of this article.)

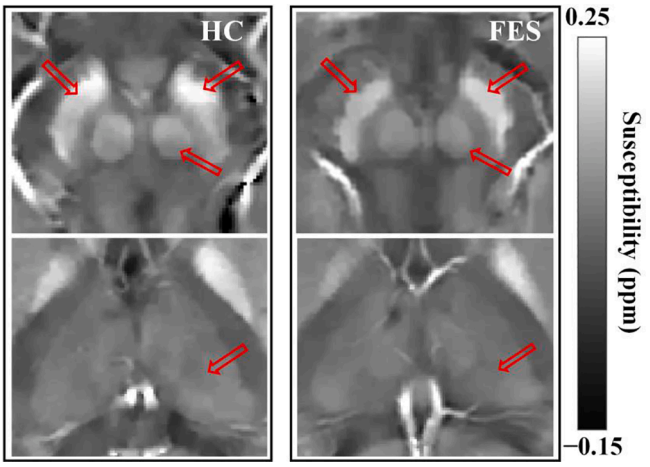

Fig. 4. Representative QSM maps of two same age individuals, a HC subject (left column) and a first-episode schizophrenia patient (right column). Note decreased susceptibility (less paramagnetic) in the deep GM nuclei in the patient. FES, first-episode schizophrenia; HC, healthy control.

of normal brain were significantly positive correlated with the previously published iron concentrations (Hallgren and Sourander, 1958; He et al., 2015; Yao et al., 2017). In addition, absolute ICCs of QSM values indicated excellent inter-rater reliability agreement in the present study. These findings confirmed the feasibility of QSM for iron quantification in the brain.

In the current study, QSM demonstrated higher sensitivity and specificity than R_2* mapping in evaluating iron alterations, enabling the detection of changes already present in patients with first-episode schizophrenia. Higher sensitivity of QSM for iron changes has also been found in other disorders such as multiple sclerosis (Blazejewska et al., 2015; Langkammer et al., 2013) and Parkinson's disease (He et al., 2015; Langkammer et al., 2016). In terms of magnetic susceptibility physics, the attenuation rate of the exponential R_2* reflecting the static dephasing by the inhomogeneous field plus the random dephasing, is geometrically dependent on the iron concentration (Yablonskiy and Haacke, 1994). The inhomogeneous field estimated from the MRI signal is the tissue susceptibility convolved with a dipole kernel. The deconvolution of the field map produces QSM, which is then divided by the molar susceptibility of iron to obtain the iron concentration map (Liu et al., 2012; Murakami et al., 2015; Rochefort et al., 2010). This deconvolution process can eliminate the blooming artifacts that are unavoidable in R_2*.

The results of this study showed that QSM values in all ROIs were decreased to some extent, indicating a reduction of iron concentration in these regions. Several studies have reported a link between iron deficiency and schizophrenia. Recently, Kim et al. found that iron deficiency has an effect on negative symptoms in patients with schizophrenia (Kim et al., 2018). Famitafreshi et al. impaired the iron metabolism in prefrontal cortex and hippocampus with social isolation and induced the emergence of schizophrenic-like symptoms in male rats (Famitafreshi and Karimian, 2020). Prospective studies have reported a significant association between maternal iron deficiency and the risk of schizophrenia spectrum disorders in offspring (Insel et al., 2008; Sorensen et al., 2011). Reductions of iron supply in developing brain may have long-term neural and behavioral effects (Felt et al., 2006; Lozoff et al., 2006; Unger et al., 2007), and the neurological impairments in infants caused by systemic iron deficiency persist despite iron supplementation (Beard, 2007, 2008). Takahashi et al. found profound disruptions of myelin and oligodendrocyte (Lee et al., 2013; Takahashi et al., 2011) in schizophrenia patients, which were linked to dopamine and glutamate abnormalities. Notably, iron is not only an essential cofactor of myelin synthesis but also a coenzyme of dopamine and glutamate synthesis, affecting the activity of neurotransmitter receptors (Beard and Connor, 2003). The decreased iron concentration in the GM nuclei could be implicated in the pathogenesis of schizophrenia.

The significant reduction of iron concentration in bilateral SN may be related to the dysregulation of presynaptic striatal dopamine neurotransmitter in first-episode schizophrenia patients. The nigrostriatal system, which connects the SN and the striatum (including CN, PUT and

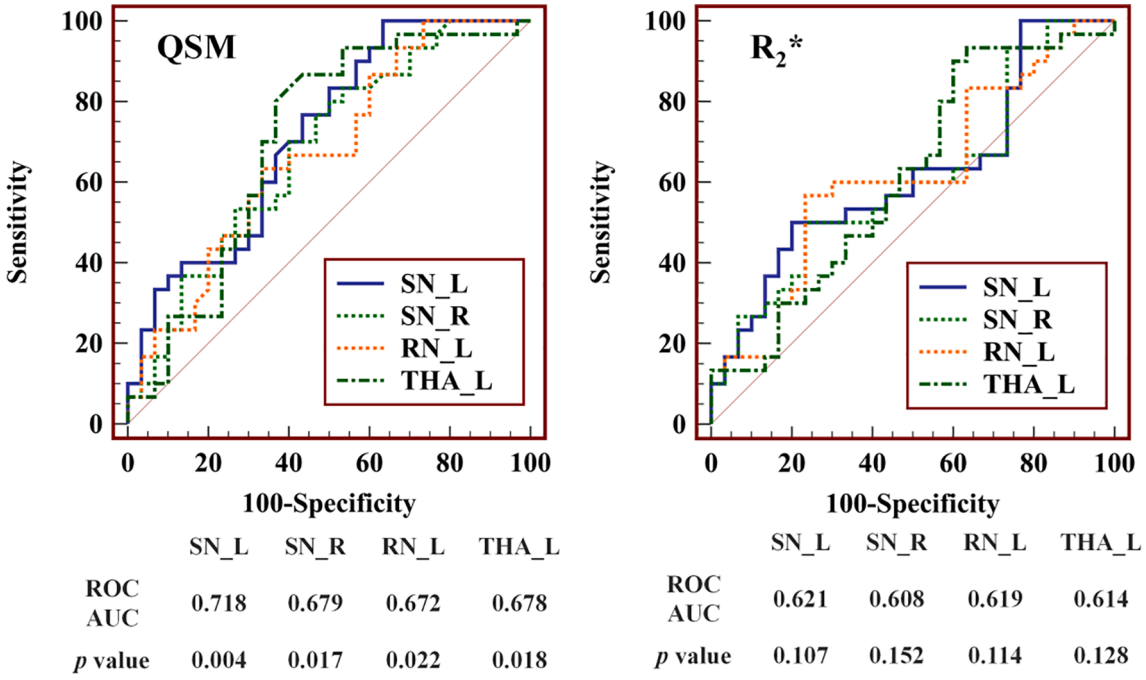

	SN_L	SN_R	RN_L	THA_L
ROC AUC	0.718	0.679	0.672	0.678
p value	0.004	0.017	0.022	0.018

	SN_L	SN_R	RN_L	THA_L
ROC AUC	0.621	0.608	0.619	0.614
p value	0.107	0.152	0.114	0.128

Fig. 5. Results of ROC curve analyses of QSM (left) and R_2* (right) values obtained from the nuclei that showed significant inter-group differences. QSM in the left SN provide highest diagnostic performance to differentiate first-episode schizophrenia patients from healthy controls. ROC, receiver operating characteristic, AUC, area under curve; SN, substantia nigra; RN, red nucleus; THA, thalamus. (For interpretation of the references to color in this figure legend, the reader is referred to the web version of this article.)

Table 4
Results of the partial correlation analyses of QSM and R_2* values in first-episode schizophrenia patients.

PANSS		QSM				R_2*			
		Left SN	Right SN	Left RN	Left THA	Left SN	Right SN	Left RN	Left THA
P	*r* value	−0.204	−0.141	−0.036	−0.038	−0.408	−0.320	−0.173	−0.420
	p value	0.572	0.698	0.922	0.917	0.241	0.368	0.633	0.226
N	*r* value	0.326	0.167	0.272	0.201	0.252	0.429	0.249	0.125
	p value	0.357	0.644	0.447	0.578	0.482	0.216	0.488	0.731
G	*r* value	0.347	0.303	0.429	0.196	0.497	0.503	0.328	0.185
	p value	0.326	0.394	0.216	0.588	0.144	0.053	0.354	0.609
T	*r* value	0.253	0.180	0.357	0.191	0.193	0.442	0.219	−0.050
	p value	0.481	0.618	0.312	0.598	0.594	0.201	0.543	0.890

SN, substantia nigra; RN, red nucleus; THA, thalamus; PANSS, Positive and Negative Syndrome Scale; P, positive symptom score; N, negative symptom score; G, general psychopathology score; T, total score.

GP), is an essential pathway in dopamine transmission (McCutcheon et al., 2019). The type 2 (D2) receptor on the dopamine nerve ending, known as the presynaptic dopamine receptor, is widely present in the nigrostriatal pathway. Some studies have reported that as the D2 receptor is an iron-containing protein, iron deficiency would result in reduced activity and attenuated affinity of D2 receptor (Erikson et al., 2001; Kim et al., 2018; Pino et al., 2017; Youdim et al., 1989). Since D2 receptor regulates dopamine uptake in the synaptic cleft through the dopamine transporter (DAT) (Meiergerd et al., 1993; Vallone et al., 2000), the negative effect of iron deficiency on D2 receptor would cause a decrease in DAT activity and density. The positive correlation between D2 density and DAT density support the possibility (Erikson et al., 2001). The decreased activity and density of DAT may cause elevated extracellular dopamine concentration in the striatum (Erikson et al., 2000). Several iron deficiency models showed reduced neuronal uptake and increased extracellular concentration of catecholaminergic neurotransmitters (Bianco et al., 2008; Burhans et al., 2005; Hare et al., 2013). Moreover, molecular imaging studies revealed that presynaptic striatal dopaminergic function is elevated in schizophrenia (Hietala et al., 1995; Howes et al., 2009; Meyer-Lindenberg et al., 2002; Moore et al., 2003). In the present study, the reduction of iron concentration in the nuclei at one end of the nigrostriatal pathway may be associated with the dopamine hypothesis in schizophrenia.

The significant reduction of iron concentration in the left THA and left RN may be related to the dysregulation of the glutamatergic receptors and neurotransmitters in first-episode schizophrenia patients. Most thalamic afferent and efferent neurotransmitters belong to the glutamatergic system (Ibrahim et al., 2000). The expression and specific binding of the N-methyl-D-aspartate (NMDA) subtype of glutamate receptors was found to be reduced in iron-deficient states (Rao et al., 2003). The decreased stimulation of hypoactive NMDA receptors on GABAergic interneurons causes an insufficient release of GABA. Since the inhibitory effect of GABA neurons on glutamate neurons is attenuated, the disinhibited glutamate neurons release abnormally high glutamate, thereby causing excitotoxic stress (Konradi and Heckers, 2003; Lewis and Moghaddam, 2006; Olney et al., 1999). Previous study reported a low NMDA receptor expression in the thalamic areas (Ibrahim et al., 2000), and a broad elevation of glutamate metabolites in the thalamus and basal ganglia of schizophrenia patients (Merritt et al., 2016; Yang et al., 2019). An animal model study of schizophrenia with NMDA receptor hypofunction observed obvious metabolic alterations of glutamatergic and GABAergic systems in areas of the cortico-striato-thalamo-cortical loop (Eyjolfsson et al., 2011). In addition, Kirsten et al. repeatedly reported increased glutamate in the left thalamus of schizophrenia patients (Kirsten et al., 2018, 2017). The RN is known to contain measurable amounts of glutamatergic and GABAergic neurons and receives the glutamatergic fibers from dentate nucleus of the cerebellum (Hernandez-Ceron et al., 2017; Nieoullon et al., 1988). The hypoactive GABAergic interneurons and hyperactive glutamate neurons have been demonstrated in the cerebellar cortices of patients with schizophrenia (Bullock et al., 2008; Paz et al., 2006). Previous studies considered that the RN might be the functional intersection point between striato-thalamo-cortical and cerebello-thalamo-cortical circuits, both of which are thought to be involved in the pathophysiology of schizophrenia (Lewis et al., 2013; Yeganeh-Doost et al., 2011). The reduced iron concentrations in thalamus and red nucleus found in the present study may be associated with the glutamate hypothesis in schizophrenia.

In the present study, the volume of bilateral PUT and SN was significantly increased in patients with first-episode schizophrenia. Previous studies have revealed volumetric alterations in the subcortical regions in schizophrenia. A large-scale multisite *meta*-analysis confirmed that patients with schizophrenia exhibited significantly larger bilateral PUT volumes, compared with controls (Okada et al., 2016). Glahn et al. reported increased volumes of the bilateral PUT and right head of the CN (Glahn et al., 2008). Moreover, Mamah et al. reported enlarged volumes in the bilateral PUT and CN and a positive correlation between attention/vigilance cognition with PUT and CN volumes in schizophrenia (Mamah et al., 2007). Regarding the SN volume of schizophrenia, no prior researches have been found to directly support the increase in volume. In a related autopsy study, Williams et al. examined the cytoarchitecture of dopaminergic neurons in the SN, and they observed increased nuclear and nucleolar size and decreased astrocyte density in schizophrenia compared to matched controls (Williams et al., 2014). An animal model study demonstrated that there exist strong positive correlations between QSM value and the density of neurons plus neuroglia cells (Gong et al., 2020). We suggested that the increased volumes and decreased QSM values of bilateral SN in the first-episode schizophrenia patients may be associated with the decreased density of ferritin-containing cells.

Altered lateralization in schizophrenia has recently been investigated. The lateralization of the brain is considered highly correlated with human behavioral and psychological characteristics (Toga and Thompson, 2003). The above-mentioned *meta*-analysis found a schizophrenia-specific leftward asymmetry in the GP volume (Okada et al., 2016). He et al. reported an increased left laterality of striatum volume in schizophrenic subjects (He et al., 2021). Maier et al. found the metabolite concentrations in schizophrenia group showed a significant left-sided reduction (Maier et al., 2000). These findings provided preliminary suggestion of the aberrant lateralization in the left neural pathway in schizophrenic. The results of this study mainly reflected in the abnormality of iron concentration in the left nuclei, suggesting a left laterality of iron reduction in patients with first-episode schizophrenia.

This study had several limitations. First, the current work focused on the susceptibility determined by the paramagnetic iron-load ferritin in the deep GM, while the white matter susceptibility could also contribute to the understanding of schizophrenia. The susceptibility in white matter has been found to be anisotropic (Li et al., 2012b; Sukstanskii and

Yablonskiy, 2014), and the explanation of the susceptibility changes in white matter is more complicated since the diamagnetic effect of myelin has to be distinguished from the paramagnetism of iron (Langkammer et al., 2013; Liu et al., 2011a). Second, this study is limited by the relatively small number of patients and controls. Therefore, a large sample size is needed in the future to verify the conclusions. Third, this study did not find a significant association between reduced iron concentration and disease severity scores. In future studies, other clinical evaluation indicators should be employed to further explore the correlation with iron deficiency in an increased sample size. Fourthly, more comprehensive clinical information, such as serum ferritin and disease course, should be collected in the future research. Moreover, the current study is a cross-sectional research. The QSM quantitation enables a longitudinal investigation to clarify the relationship between brain iron status and follow-up treatment of schizophrenia.

5. Conclusions

QSM values was decreased in bilateral substantia nigra, left red nucleus, and left thalamus in first-episode schizophrenia patients, indicating the reduction of iron concentrations in these regions. We suggest that decreased iron concentrations in these deep grey matter nuclei may be associated with the dopamine hypothesis and glutamate hypothesis of schizophrenia, respectively. In addition, QSM showed more potential for quantitative evaluation of disease-related iron changes in deep grey matter nuclei than R_2* mapping. The disturbance of iron concentration reflected by QSM may be a potential biomarker for further understanding the pathophysiological mechanism of first-episode schizophrenia.

CRediT authorship contribution statement

Man Xu: Conceptualization, Data curation, Formal analysis, Investigation, Methodology, Visualization, Writing - original draft, Writing - review & editing. **Yihao Guo:** Conceptualization, Investigation, Methodology, Writing - review & editing. **Junying Cheng:** Funding acquisition, Methodology, Software. **Kangkang Xue:** Data curation, Formal analysis. **Meng Yang:** Data curation, Investigation. **Xueqin Song:** Conceptualization, Resources. **Yanqiu Feng:** Conceptualization, Project administration, Supervision, Writing - review & editing. **Jingliang Cheng:** Funding acquisition, Project administration, Validation.

Declaration of Competing Interest

The authors declare that they have no known competing financial interests or personal relationships that could have appeared to influence the work reported in this paper.

Acknowledgements

This work was supported by the National Natural Science Foundation of China (No. 81871327) and the Union Project of Medical and Technology Research Program of Henan Province (No. LHG20190159).

References

Barbosa, J.H.O., Santos, A.C., Tumas, V., Liu, M., Zheng, W., Haacke, E.M., Salmon, C.E. G., 2015. Quantifying brain iron deposition in patients with Parkinson's disease using quantitative susceptibility mapping, R2 and R2*. Magn. Reson. Imaging 33, 559–565. https://doi.org/10.1016/j.mri.2015.02.021.

Beard, J.L., 2007. Recent evidence from human and animal studies regarding iron status and infant development. J. Nutr. 137, 524S–530S. https://doi.org/10.1093/jn/137.2.524S.

Beard, J.L., 2008. Why iron deficiency is important in infant development. J. Nutr. 138, 2534–2536. https://doi.org/10.1093/jn/138.12.2534.

Beard, J.L., Connor, J.R., 2003. Iron status and neural functioning. Annu. Rev. Nutr. 23, 41–58. https://doi.org/10.1146/annurev.nutr.23.020102.075739.

Bianco, L.E., Wiesinger, J., Earley, C.J., Jones, B.C., Beard, J.L., 2008. Iron deficiency alters dopamine uptake and response to L-DOPA injection in Sprague-Dawley rats. J. Neurochem. 106, 205–215. https://doi.org/10.1111/j.1471-4159.2008.05358.x.

Blazejewska, A.I., Al-Radaideh, A.M., Wharton, S., Lim, S.Y., Bowtell, R.W., Constantinescu, C.S., Gowland, P.A., 2015. Increase in the iron content of the substantia nigra and red nucleus in multiple sclerosis and clinically isolated syndrome: a 7 Tesla MRI study. J. Magn. Reson. Imaging 41, 1065–1070. https://doi.org/10.1002/jmri.24644.

Bullock, W.M., Cardon, K., Bustillo, J., Roberts, R.C., Perrone-Bizzozero, N.I., 2008. Altered expression of genes involved in GABAergic transmission and neuromodulation of granule cell activity in the cerebellum of schizophrenia patients. Am. J. Psychiatry 165, 1594–1603. https://doi.org/10.1176/appi.ajp.2008.07121845.

Burhans, M.S., Dailey, C., Beard, Z., Wiesinger, J., Murray-Kolb, L., Jones, B.C., Beard, J. L., 2005. Iron deficiency: differential effects on monoamine transporters. Nutr. Neurosci. 8, 31–38. https://doi.org/10.1080/10284150500047070.

Chen, L., Hua, J., Ross, C.A., Cai, S., van Zijl, P.C.M., Li, X., 2019. Altered brain iron content and deposition rate in Huntington's disease as indicated by quantitative susceptibility MRI. J. Neurosci. Res. 97 (4), 467–479. https://doi.org/10.1002/jnr.24358.

Crichton, R.R., Dexter, D.T., Ward, R.J., 2011. Brain iron metabolism and its perturbation in neurological diseases. J. Neural Transm. (Vienna) 118, 301–314. https://doi.org/10.1007/s00702-010-0470-z.

Cristina, Sánchez-Castañeda, Ferdinando, Squitieri, Margherita, Di, Paola, Michael, Dayan, Martina, 2015. The role of iron in gray matter degeneration in Huntington's disease: a magnetic resonance imaging study. Hum. Brain Mapp. 36 (1), 50–66. https://doi.org/10.1002/hbm.22612.

Erikson, K.M., Jones, B.C., Beard, J.L., 2000. Iron deficiency alters dopamine transporter functioning in rat striatum. J. Nutr. 130, 2831–2837. https://doi.org/10.1093/jn/130.11.2831.

Erikson, K.M., Jones, B.C., Hess, E.J., Zhang, Q., Beard, J.L., 2001. Iron deficiency decreases dopamine D1 and D2 receptors in rat brain. Pharmacol. Biochem. Behav. 69, 409–418. https://doi.org/10.1016/s0091-3057(01)00563-9.

Eskreis-Winkler, S., Zhang, Y., Zhang, J., Liu, Z., Dimov, A., Gupta, A., Wang, Y., 2017. The clinical utility of QSM: disease diagnosis, medical management, and surgical planning. NMR Biomed. 30 https://doi.org/10.1002/nbm.3668.

Eyjolfsson, E.M., Nilsen, L.H., Kondziella, D., Brenner, E., Haberg, A., Sonnewald, U., 2011. Altered 13C glucose metabolism in the cortico-striato-thalamo-cortical loop in the MK-801 rat model of schizophrenia. J. Cereb. Blood Flow Metab. 31, 976–985. https://doi.org/10.1038/jcbfm.2010.193.

Famitafreshi, H., Karimian, M., 2020. Paradoxical regulation of iron in hippocampus and prefrontal cortex induces schizophrenic-like symptoms in male rats. Int. J. Neurosci. 130, 384–390. https://doi.org/10.1080/00207454.2019.1692832.

Felt, B.T., Beard, J.L., Schallert, T., Shao, J., Aldridge, J.W., Connor, J.R., Georgieff, M. K., Lozoff, B., 2006. Persistent neurochemical and behavioral abnormalities in adulthood despite early iron supplementation for perinatal iron deficiency anemia in rats. Behav. Brain Res. 171, 261–270. https://doi.org/10.1016/j.bbr.2006.04.001.

Ganz, T., Nemeth, E., 2006. Regulation of iron acquisition and iron distribution in mammals. Biochim. Biophys. Acta 1763, 690–699. https://doi.org/10.1016/j.bbamcr.2006.03.014.

Glahn, D.C., Laird, A.R., Ellison-Wright, I., Thelen, S.M., Robinson, J.L., Lancaster, J.L., Bullmore, E., Fox, P.T., 2008. Meta-analysis of gray matter anomalies in schizophrenia: application of anatomic likelihood estimation and network analysis. Biol. Psychiatry 64, 774–781. https://doi.org/10.1016/j.biopsych.2008.03.031.

Goff, D.C., Coyle, J.T., 2001. The emerging role of glutamate in the pathophysiology and treatment of schizophrenia. Am. J. Psychiatry 158, 1367–1377. https://doi.org/10.1176/appi.ajp.158.9.1367.

Gong, N.J., Dibb, R., Pletnikov, M., Benner, E., Liu, C., 2020. Imaging microstructure with diffusion and susceptibility MR: neuronal density correlation in Disrupted-in-Schizophrenia-1 mutant mice. NMR Biomed. 33, e4365 https://doi.org/10.1002/nbm.4365.

Haacke, E.M., Cheng, N.Y.C., House, M.J., Liu, Q., Neelavalli, J., Ogg, R.J., Khan, A., Ayaz, M., Kirsch, W., Obenaus, A., 2005. Imaging iron stores in the brain using magnetic resonance imaging. Magn. Reson. Imaging 23, 1–25. https://doi.org/10.1016/j.mri.2004.10.001.

Hallgren, B., Sourander, P., 1958. The effect of age on the non-haemin iron in the human brain. J. Neurochem. 3, 41–51. https://doi.org/10.1111/j.1471-4159.1958.tb12607.x.

Hare, D., Ayton, S., Bush, A., Lei, P., 2013. A delicate balance: Iron metabolism and diseases of the brain. Front. Aging Neurosci. 5, 34. https://doi.org/10.3389/fnagi.2013.00034.

Hare, D.J., Double, K.L., 2016. Iron and dopamine: a toxic couple. Brain 139, 1026–1035. https://doi.org/10.1093/brain/aww022.

He, H., Luo, C., Li, N., Li, Z., Duan, M., Yao, G., Wang, H., He, M., Yao, D., 2021. Altered asymmetries of diffusion and volumetry in basal ganglia of schizophrenia. Brain Imaging Behav. 15, 782–787. https://doi.org/10.1007/s11682-020-00286-7.

He, N., Ling, H., Ding, B., Huang, J., Zhang, Y., Zhang, Z., Liu, C., Chen, K., Yan, F., 2015. Region-specific disturbed iron distribution in early idiopathic Parkinson's disease measured by quantitative susceptibility mapping. Hum. Brain Mapp. 36, 4407–4420. https://doi.org/10.1002/hbm.22928.

Hernandez-Ceron, M., Martinez-Lazcano, J.C., Rubio, C., Custodio, V., Gonzalez-Guevara, E., Castillo-Perez, C., Paz, C., 2017. Participation of the dentate-rubral pathway in the kindling model of epilepsy. J. Neurosci. Res. 95, 1495–1502. https://doi.org/10.1002/jnr.23974.

Hietala, J., Syvalahti, E., Vuorio, K., Rakkolainen, V., Bergman, J., Haaparanta, M., Solin, O., Kuoppamaki, M., Kirvela, O., Ruotsalainen, U., et al., 1995. Presynaptic

dopamine function in striatum of neuroleptic-naive schizophrenic patients. Lancet 346, 1130–1131. https://doi.org/10.1016/s0140-6736(95)91801-9.
Howes, O.D., Kapur, S., 2009. The dopamine hypothesis of schizophrenia: version III–the final common pathway. Schizophr. Bull. 35, 549–562. https://doi.org/10.1093/schbul/sbp006.
Howes, O.D., Montgomery, A.J., Asselin, M.C., Murray, R.M., Valli, I., Tabraham, P., Bramon-Bosch, E., Valmaggia, L., Johns, L., Broome, M., McGuire, P.K., Grasby, P. M., 2009. Elevated striatal dopamine function linked to prodromal signs of schizophrenia. Arch. Gen. Psychiatry 66, 13–20. https://doi.org/10.1001/archgenpsychiatry.2008.514.
Hyacinthe, C., De Deurwaerdere, P., Thiollier, T., Li, Q., Bezard, E., Ghorayeb, I., 2015. Blood withdrawal affects iron store dynamics in primates with consequences on monoaminergic system function. Neuroscience 290, 621–635. https://doi.org/10.1016/j.neuroscience.2015.01.057.
Ibrahim, H.M., Hogg Jr., A.J., Healy, D.J., Haroutunian, V., Davis, K.L., Meador-Woodruff, J.H., 2000. Ionotropic glutamate receptor binding and subunit mRNA expression in thalamic nuclei in schizophrenia. Am. J. Psychiatry 157, 1811–1823. https://doi.org/10.1176/appi.ajp.157.11.1811.
Insel, B.J., Schaefer, C.A., McKeague, I.W., Susser, E.S., Brown, A.S., 2008. Maternal iron deficiency and the risk of schizophrenia in offspring. Arch. Gen. Psychiatry 65, 1136–1144. https://doi.org/10.1001/archpsyc.65.10.1136.
Jing, S., Qingbao, Y., Hao, H., Pearlson, G.D., Calhoun, V.D., 2012. A selective review of multimodal fusion methods in Schizophrenia. Front. Hum. Neurosci. 6 https://doi.org/10.3389/fnhum.2012.00027.
Khalil, M., Enzinger, C., Langkammer, C., Tscherner, M., Fazekas, F., 2009. Quantitative assessment of brain iron by R(2)* relaxometry in patients with clinically isolated syndrome and relapsing-remitting multiple sclerosis. Mult. Scler. 15, 1048–1054. https://doi.org/10.1177/1352458509106609.
Khalil, M., Langkammer, C., Ropele, S., Petrovic, K., Wallner-Blazek, M., Loitfelder, M., Jehna, M., Bachmaier, G., Schmidt, R., Enzinger, C., Fuchs, S., Fazekas, F., 2011. Determinants of brain iron in multiple sclerosis: a quantitative 3T MRI study. Neurology 77, 1691–1697. https://doi.org/10.1212/WNL.0b013e318236ef0e.
Kim, S.-W., Stewart, R., Park, W.-Y., Jhon, M., Lee, J.-Y., Kim, S.-Y., Kim, J.-M., Amminger, P., Chung, Y.-C., Yoon, J.-S., 2018. Latent iron deficiency as a marker of negative symptoms in patients with first-episode schizophrenia spectrum disorder. Nutrients 10, 1707. https://doi.org/10.3390/nu10111707.
Kirsten, B., Brian, B., Kasper, J., Anne, S., Karen, T., Degaard, N.M., Egill, R., Birte, G., 2018. F16. Glutamate and gaba levels in antipsychotic-naïve schizophrenia patients are associated with treatment outcome after 1.5 and 6 months. Schizophr. Bull. S224–S225 https://doi.org/10.1093/schbul/sby017.547.
Kirsten, B., Kasper, J., Anne, S., Jensen, M.B., Egill, R., Broberg, B.V., Glenthj, B.Y., 2017. 87. Glutamate and GABA in Antipsychotic-Naive Schizophrenia and Association With Treatment Outcome. Schizophr. Bull. https://doi.org/10.1093/schbul/sbx021.126. S48-S48.
Konradi, C., Heckers, S., 2003. Molecular aspects of glutamate dysregulation: implications for schizophrenia and its treatment. Pharmacol. Ther. 97, 153–179. https://doi.org/10.1016/s0163-7258(02)00328-5.
Langkammer, C., Krebs, N., Goessler, W., Scheurer, E., Ebner, F., Yen, K., Fazekas, F., Ropele, S., 2010. Quantitative MR imaging of brain iron: a postmortem validation study. Radiology 257, 455–462. https://doi.org/10.1148/radiol.10100495.
Langkammer, C., Liu, T., Khalil, M., Enzinger, C., Jehna, M., Fuchs, S., Fazekas, F., Wang, Y., Ropele, S., 2013. Quantitative susceptibility mapping in multiple sclerosis. Radiology 267, 551–559. https://doi.org/10.1148/radiol.12120707.
Langkammer, C., Pirpamer, L., Seiler, S., Deistung, A., Schweser, F., Franthal, S., Homayoon, N., Katschnig-Winter, P., Koegl-Wallner, M., Pendl, T., Stoegerer, E.M., Wenzel, K., Fazekas, F., Ropele, S., Reichenbach, J.R., Schmidt, R., Schwingenschuh, P., 2016. Quantitative susceptibility mapping in Parkinson's disease. PLoS One 11, e0162460. https://doi.org/10.1371/journal.pone.0162460.
Langkammer, C., Schweser, F., Krebs, N., Deistung, A., Goessler, W., Scheurer, E., Sommer, K., Reishofer, G., Yen, K., Fazekas, F., Ropele, S., Reichenbach, J.R., 2012. Quantitative susceptibility mapping (QSM) as a means to measure brain iron? A post mortem validation study. NeuroImage. 62, 1593–1599. https://doi.org/10.1016/j.neuroimage.2012.05.049.
Lee, S.H., Kubicki, M., Asami, T., Seidman, L.J., Goldstein, J.M., Mesholam-Gately, R.I., Mccarley, R.W., Shenton, M.E., 2013. Extensive white matter abnormalities in patients with first-episode schizophrenia: a Diffusion Tensor Iimaging (DTI) study. Schizophr. Res. 143, 231–238. https://doi.org/10.1016/j.schres.2012.11.029.
Lewis, D.A., Moghaddam, B., 2006. Cognitive dysfunction in schizophrenia: convergence of gamma-aminobutyric acid and glutamate alterations. Arch Neurol. 63, 1372–1376. https://doi.org/10.1001/archneur.63.10.1372.
Lewis, M.M., Du, G., Kidacki, M., Patel, N., Shaffer, M.L., Mailman, R.B., Huang, X., 2013. Higher iron in the red nucleus marks Parkinson's dyskinesia. Neurobiol Aging 34, 1497–1503. https://doi.org/10.1016/j.neurobiolaging.2012.10.025.
Li, J., Chang, S., Liu, T., Wang, Q., Cui, D., Chen, X., Jin, M., Wang, B., Pei, M., Wisnieff, C., Spincemaille, P., Zhang, M., Wang, Y., 2012a. Reducing the object orientation dependence of susceptibility effects in gradient echo MRI through quantitative susceptibility mapping. Magn. Reson. Med. 68, 1563–1569. https://doi.org/10.1002/mrm.24135.
Li, W., Wu, B., Avram, A.V., Liu, C., 2012b. Magnetic susceptibility anisotropy of human brain in vivo and its molecular underpinnings. NeuroImage 59, 2088–2097. https://doi.org/10.1016/j.neuroimage.2011.10.038.
Li, W., Wu, B., Batrachenko, A., Bancroft-Wu, V., Morey, R.A., Shashi, V., Langkammer, C., De Bellis, M.D., Ropele, S., Song, A.W., Liu, C., 2014. Differential developmental trajectories of magnetic susceptibility in human brain gray and white matter over the lifespan. Hum. Brain Mapp. 35, 2698–2713. https://doi.org/10.1002/hbm.22360.
Li, W., Wu, B., Liu, C., 2011. Quantitative susceptibility mapping of human brain reflects spatial variation in tissue composition. NeuroImage 55, 1645–1656. https://doi.org/10.1016/j.neuroimage.2010.11.088.
Liu, C., Li, W., Johnson, G.A., Wu, B., 2011a. High-field (9.4 T) MRI of brain dysmyelination by quantitative mapping of magnetic susceptibility. NeuroImage 56, 930–938. https://doi.org/10.1016/j.neuroimage.2011.02.024.
Liu, C., Li, W., Tong, K.A., Yeom, K.W., Kuzminski, S., 2015. Susceptibility-weighted imaging and quantitative susceptibility mapping in the brain. J. Magn. Reson. Imaging 42, 23–41. https://doi.org/10.1002/jmri.24768.
Liu, J., Liu, T., Rochefort, L.D., Ledoux, J., Khalidov, I., Chen, W., Tsiouris, A.J., Wisnieff, C., Spincemaille, P., Prince, M.R., 2012. Morphology enabled dipole inversion for quantitative susceptibility mapping using structural consistency between the magnitude image and the susceptibility map. NeuroImage 59, 2560–2568. https://doi.org/10.1016/j.neuroimage.2011.08.082.
Liu, T., Liu, J., de Rochefort, L., Spincemaille, P., Khalidov, I., Ledoux, J.R., Wang, Y., 2011b. Morphology enabled dipole inversion (MEDI) from a single-angle acquisition: comparison with COSMOS in human brain imaging. Magn. Reson. Med. 66, 777–783. https://doi.org/10.1002/mrm.22816.
Lozoff, B., Beard, J., Connor, J., Barbara, F., Georgieff, M., Schallert, T., 2006. Long-lasting neural and behavioral effects of iron deficiency in infancy. Nutr Rev. 64, S34-43; discussion S72-91. 10.1301/nr.2006.may.s34-s43.
Lyne, J., Kelly, B.D., O'Connor, W.T., 2004. Schizophrenia: a review of neuropharmacology. Ir. J. Med. Sci. 173, 155–159. https://doi.org/10.1007/BF03167931.
Maier, M., Mellers, J., Toone, B., Trimble, M., Ron, M.A., 2000. Schizophrenia, temporal lobe epilepsy and psychosis: an in vivo magnetic resonance spectroscopy and imaging study of the hippocampus/amygdala complex. Psychol. Med. 30, 571–581. https://doi.org/10.1017/s0033291799001993.
Mamah, D., Wang, L., Barch, D., de Erausquin, G.A., Gado, M., Csernansky, J.G., 2007. Structural analysis of the basal ganglia in schizophrenia. Schizophr. Res. 89, 59–71. https://doi.org/10.1016/j.schres.2006.08.031.
McCutcheon, R.A., Abi-Dargham, A., Howes, O.D., 2019. Schizophrenia, dopamine and the striatum: from biology to symptoms. Trends Neurosci. 42, 205–220. https://doi.org/10.1016/j.tins.2018.12.004.
Meiergerd, S.M., Patterson, T.A., Schenk, J.O., 1993. D2 receptors may modulate the function of the striatal transporter for dopamine: kinetic evidence from studies in vitro and in vivo. J. Neurochem. 61, 764–767. https://doi.org/10.1111/j.1471-4159.1993.tb02185.x.
Merritt, K., Egerton, A., Kempton, M.J., Taylor, M.J., McGuire, P.K., 2016. Nature of glutamate alterations in schizophrenia: a meta-analysis of proton magnetic resonance spectroscopy studies. JAMA Psychiatry 73, 665–674. https://doi.org/10.1001/jamapsychiatry.2016.0442.
Meyer-Lindenberg, A., Miletich, R.S., Kohn, P.D., Esposito, G., Carson, R.E., Quarantelli, M., Weinberger, D.R., Berman, K.F., 2002. Reduced prefrontal activity predicts exaggerated striatal dopaminergic function in schizophrenia. Nat. Neurosci. 5, 267–271. https://doi.org/10.1038/nn804.
Moore, R.Y., Whone, A.L., McGowan, S., Brooks, D.J., 2003. Monoamine neuron innervation of the normal human brain: an 18F-DOPA PET study. Brain Res. 982, 137–145. https://doi.org/10.1016/s0006-8993(03)02721-5.
Moos, T., Morgan, E.H., 2004. The metabolism of neuronal iron and its pathogenic role in neurological disease: review. Ann. N. Y. Acad. Sci. 1012, 14–26. https://doi.org/10.1196/annals.1306.002.
Murakami, Y., Kakeda, S., Watanabe, K., Ueda, I., Ogasawara, A., Moriya, J., Ide, S., Futatsuya, K., Sato, T., Okada, K., Uozumi, T., Tsuji, S., Liu, T., Wang, Y., Korogi, Y., 2015. Usefulness of quantitative susceptibility mapping for the diagnosis of Parkinson disease. AJNR Am. J. Neuroradiol. 36, 1102–1108. https://doi.org/10.3174/ajnr.A4260.
Nielsen, P., Gunther, U., Durken, M., Fischer, R., Dullmann, J., 2000. Serum ferritin iron in iron overload and liver damage: correlation to body iron stores and diagnostic relevance. J. Lab. Clin. Med. 135, 413–418. https://doi.org/10.1067/mlc.2000.106456.
Nieoullon, A., Vuillon-Cacciuttolo, G., Dusticier, N., Kerkerian, L., Andre, D., Bosler, O., 1988. Putative neurotransmitters in the red nucleus and their involvement in postlesion adaptive mechanisms. Behav. Brain Res. 28, 163–174. https://doi.org/10.1016/0166-4328(88)90093-9.
Okada, N., Fukunaga, M., Yamashita, F., Koshiyama, D., Yamamori, H., Ohi, K., Yasuda, Y., Fujimoto, M., Watanabe, Y., Yahata, N., Nemoto, K., Hibar, D.P., van Erp, T.G., Fujino, H., Isobe, M., Isomura, S., Natsubori, T., Narita, H., Hashimoto, N., Miyata, J., Koike, S., Takahashi, T., Yamasue, H., Matsuo, K., Onitsuka, T., Iidaka, T., Kawasaki, Y., Yoshimura, R., Watanabe, Y., Suzuki, M., Turner, J.A., Takeda, M., Thompson, P.M., Ozaki, N., Kasai, K., Hashimoto, R., 2016. Abnormal asymmetries in subcortical brain volume in schizophrenia. Mol. Psychiatry 21, 1460–1466. https://doi.org/10.1038/mp.2015.209.
Olney, J.W., Newcomer, J.W., Farber, N.B., 1999. NMDA receptor hypofunction model of schizophrenia. J. Psychiatr. Res. 33, 523–533. https://doi.org/10.1016/s0022-3956(99)00029-1.
Paz, R.D., Andreasen, N.C., Daoud, S.Z., Conley, R., Roberts, R., Bustillo, J., Perrone-Bizzozero, N.I., 2006. Increased expression of activity-dependent genes in cerebellar glutamatergic neurons of patients with schizophrenia. Am. J. Psychiatry 163, 1829–1831. https://doi.org/10.1176/ajp.2006.163.10.1829.
Pei, M., Nguyen, T.D., Thimmappa, N.D., Salustri, C., Dong, F., Cooper, M.A., Li, J., Prince, M.R., Wang, Y., 2015. Algorithm for fast monoexponential fitting based on Auto-Regression on Linear Operations (ARLO) of data. Magn. Reson. Med. 73, 843–850. https://doi.org/10.1002/mrm.25137.
Pino, J.M.V., da Luz, M.H.M., Antunes, H.K.M., Giampa, S.Q.C., Martins, V.R., Lee, K.S., 2017. Iron-restricted diet affects brain ferritin levels, dopamine metabolism and

cellular prion protein in a region-specific manner. Front. Mol. Neurosci. 10, 145. https://doi.org/10.3389/fnmol.2017.00145.
Ramos, P., Santos, A., Pinto, N.R., Mendes, R., Magalhaes, T., Almeida, A., 2014. Iron levels in the human brain: a post-mortem study of anatomical region differences and age-related changes. J. Trace Elem. Med. Biol. 28, 13–17. https://doi.org/10.1016/j.jtemb.2013.08.001.
Rao, R., Tkac, I., Townsend, E.L., Gruetter, R., Georgieff, M.K., 2003. Perinatal iron deficiency alters the neurochemical profile of the developing rat hippocampus. J. Nutr. 133, 3215–3221. https://doi.org/10.1093/jn/133.10.3215.
Rochefort, L.D., Liu, T., Kressler, B., Liu, J., Spincemaille, P., Lebon, V., Wu, J., Wang, Y., 2010. Quantitative susceptibility map reconstruction from MR phase data using bayesian regularization: validation and application to brain imaging. Magn. Reson. Med. 63, 194–206. https://doi.org/10.1002/mrm.22187.
Ropele, S., Langkammer, C., 2016. Iron quantification with susceptibility. NMR Biomed. 30 https://doi.org/10.1002/nbm.3534.
Rouault, T.A., 2013. Iron metabolism in the CNS: implications for neurodegenerative diseases. Nat. Rev. Neurosci. 14, 551–564. https://doi.org/10.1038/nrn3453.
Schofield, M.A., Zhu, Y., 2003. Fast phase unwrapping algorithm for interferometric applications. Opt. Lett. 28, 1194–1196. https://doi.org/10.1364/ol.28.001194.
Sorensen, H.J., Nielsen, P.R., Pedersen, C.B., Mortensen, P.B., 2011. Association between prepartum maternal iron deficiency and offspring risk of schizophrenia: population-based cohort study with linkage of Danish national registers. Schizophr. Bull. 37, 982–987. https://doi.org/10.1093/schbul/sbp167.
Stankiewicz, J., Panter, S.S., Neema, M., Arora, A., Batt, C.E., Bakshi, R., 2007. Iron in chronic brain disorders: imaging and neurotherapeutic implications. Neurotherapeutics. 4, 371–386. https://doi.org/10.1016/j.nurt.2007.05.006.
Stuber, C., Pitt, D., Wang, Y., 2016. Iron in multiple sclerosis and its noninvasive imaging with quantitative susceptibility mapping. Int. J. Mol. Sci. 17 https://doi.org/10.3390/ijms17010100.
Sukstanskii, A.L., Yablonskiy, D.A., 2014. On the role of neuronal magnetic susceptibility and structure symmetry on gradient echo MR signal formation. Magn. Reson. Med. 71, 345–353. https://doi.org/10.1002/mrm.24629.
Sun, H., Walsh, A.J., Lebel, R.M., Blevins, G., Catz, I., Lu, J.Q., Johnson, E.S., Emery, D.J., Warren, K.G., Wilman, A.H., 2015. Validation of quantitative susceptibility mapping with Perls' iron staining for subcortical gray matter. NeuroImage 105, 486–492. https://doi.org/10.1016/j.neuroimage.2014.11.010.
Takahashi, N., Sakurai, T., Davis, K.L., Buxbaum, J.D., 2011. Linking oligodendrocyte and myelin dysfunction to neurocircuitry abnormalities in schizophrenia. Prog. Neurobiol. 93, 13–24. https://doi.org/10.1016/j.pneurobio.2010.09.004.
Toga, A.W., Thompson, P.M., 2003. Mapping brain asymmetry. Nat. Rev. Neurosci. 4, 37–48. https://doi.org/10.1038/nrn1009.
Unger, E.L., Paul, T., Murray-Kolb, L.E., Felt, B., Jones, B.C., Beard, J.L., 2007. Early iron deficiency alters sensorimotor development and brain monoamines in rats. J. Nutr. 137, 118–124. https://doi.org/10.1093/jn/137.1.118.
Vallone, D., Picetti, R., Borrelli, E., 2000. Structure and function of dopamine receptors. Neurosci. Biobehav. Rev. 24, 125–132. https://doi.org/10.1016/s0149-7634(99)00063-9.
van Bergen, J.M., Hua, J., Unschuld, P.G., Lim, I.A., Jones, C.K., Margolis, R.L., Ross, C. A., van Zijl, P.C., Li, X., 2016. Quantitative susceptibility mapping suggests altered brain iron in premanifest huntington disease. AJNR Am. J. Neuroradiol. 37, 789–796. https://doi.org/10.3174/ajnr.A4617.
van Os, J., Kenis, G., Rutten, B.P., 2010. The environment and schizophrenia. Nature 468, 203–212. https://doi.org/10.1038/nature09563.
Wang, Y., Liu, T., 2015. Quantitative susceptibility mapping (QSM): Decoding MRI data for a tissue magnetic biomarker. Magn. Reson. Med. 73, 82–101. https://doi.org/10.1002/mrm.25358.
Ward, K.L., Tkac, I., Jing, Y., Felt, B., Beard, J., Connor, J., Schallert, T., Georgieff, M.K., Rao, R., 2007. Gestational and lactational iron deficiency alters the developing striatal metabolome and associated behaviors in young rats. J. Nutr. 137, 1043–1049. https://doi.org/10.1093/jn/137.4.1043.
Ward, R.J., Zucca, F.A., Duyn, J.H., Crichton, R.R., Zecca, L., 2014. The role of iron in brain ageing and neurodegenerative disorders. Lancet Neurol. 13, 1045–1060. https://doi.org/10.1016/S1474-4422(14)70117-6.
Williams, M.R., Galvin, K., O'Sullivan, B., MacDonald, C.D., Ching, E.W., Turkheimer, F., Howes, O.D., Pearce, R.K., Hirsch, S.R., Maier, M., 2014. Neuropathological changes in the substantia nigra in schizophrenia but not depression. Eur. Arch. Psychiatry Clin. Neurosci. 264, 285–296. https://doi.org/10.1007/s00406-013-0479-z.
Yablonskiy, D.A., Haacke, E.M., 1994. Theory of NMR signal behavior in magnetically inhomogeneous tissues: the static dephasing regime. Magn. Reson. Med. 32, 749–763. https://doi.org/10.1002/mrm.1910320610.
Yang, J., Guo, H., Sun, D., Duan, J., Rao, X., Xu, F., Manyande, A., Tang, Y., Wang, J., Wang, F., 2019. Elevated glutamate, glutamine and GABA levels and reduced taurine level in a schizophrenia model using an in vitro proton nuclear magnetic resonance method. Am. J. Transl. Res. 11, 5919–5931.
Yao, S., Zhong, Y., Xu, Y., Qin, J., Zhang, N., Zhu, X., Li, Y., 2017. Quantitative susceptibility mapping reveals an association between brain iron load and depression severity. Front. Hum. Neurosci. 11, 442. https://doi.org/10.3389/fnhum.2017.00442.
Yeganeh-Doost, P., Gruber, O., Falkai, P., Schmitt, A., 2011. The role of the cerebellum in schizophrenia: from cognition to molecular pathways. Clinics (Sao Paulo) 66 (Suppl 1), 71–77. https://doi.org/10.1590/s1807-59322011001300009.
Youdim, M.B., Ben-Shachar, D., Yehuda, S., 1989. Putative biological mechanisms of the effect of iron deficiency on brain biochemistry and behavior. Am J Clin Nutr. 50, 607-615; discussion 615-607. 10.1093/ajcn/50.3.607.
Yushkevich, P.A., Piven, J., Hazlett, H.C., Smith, R.G., Ho, S., Gee, J.C., Gerig, G., 2006. User-guided 3D active contour segmentation of anatomical structures: Significantly improved efficiency and reliability. NeuroImage 31, 1116–1128. https://doi.org/10.1016/j.neuroimage.2006.01.015.
Zheng, W., Monnot, A.D., 2012. Regulation of brain iron and copper homeostasis by brain barrier systems: implication in neurodegenerative diseases. Pharmacol. Ther. 133, 177–188. https://doi.org/10.1016/j.pharmthera.2011.10.006.
Zheng, W., Nichol, H., Liu, S., Cheng, Y.C., Haacke, E.M., 2013. Measuring iron in the brain using quantitative susceptibility mapping and X-ray fluorescence imaging. NeuroImage 78, 68–74. https://doi.org/10.1016/j.neuroimage.2013.04.022.
Zhou, D., Liu, T., Spincemaille, P., Wang, Y., 2014. Background field removal by solving the Laplacian boundary value problem. NMR Biomed. 27, 312–319. https://doi.org/10.1002/nbm.3064.